Pol. J. Environ. Stud. Vol. XX, No. X (XXXX), 1-13
DOI: *10.15244/pjoes/220227* ONLINE PUBLICATION DATE: 2026-09-07

Original Research

Multi-USVs Collaborative Water Pollution Traceability and Source Localization Using an Improved Wolf Pack Algorithm

Quan Zhang[1], Xiaoxiao Liu[2], Lan Zhang[1], Qian Wang[1], Kaiwei Wang[2], Tao Ding[2]*

[1]Ecological and Environmental Monitoring Center of Zhejiang Province, Hangzhou 310012, China
[2]Department of Environmental Engineering, China Jiliang University, Hangzhou 310018, China

Received: 10 December 2025
Accepted: 31 March 2026

Abstract

With the increasing frequency of water pollution incidents due to urbanization and industrialization, this paper proposes an Improved Wolf Pack Algorithm (IWPA) for coordinating multiple Unmanned Surface Vessels (USVs) to achieve rapid river pollution traceability. The IWPA incorporates a dynamic step adjustment mechanism and a dynamic population adjustment strategy to overcome the limitations of the fixed step factor and random repositioning in the standard Wolf Pack Algorithm (WPA). These enhancements prevent the algorithm from converging on local optima and improve the overall traceability efficiency of the multi-USV formation. Simulation results demonstrate the superior performance of IWPA. Under conditions of a 1500 g/s source emission rate, a 3 m/s longitudinal flow velocity, and using only 5 USVs, IWPA achieves a success rate of 97.3% and an average localization error of 0.41 m. These results represent improvements of 15.9% in success rate and 71.3% in error reduction compared to the standard WPA. Laboratory-based water pollution traceability tests further confirm the method's effectiveness, with a success rate of 80%, validating its practical localization capability.

Keywords: water pollution traceability, improved wolf pack algorithm, multi unmanned surface vessels, simulation experiment

Introduction

As a fundamental strategic resource for human survival and development, water resources play an irreplaceable role in socioeconomic advancement and ecological security. However, the distribution of water resources in China is characterized by significant regional imbalances, with declining total availability and chronically low per capita levels [1-3]. Over the past three decades, China's total water resources have continued to decrease amid rapid economic growth, with per capita availability dropping to 2,050 m^3, merely 28% of the global average. Consequently, the United Nations classifies China as a moderately water-scarce country [4-6]. Rapid urbanization and industrialization have further exacerbated water scarcity through increasing pollution incidents.

*e-mail: dingtao@cjlu.edu.cn
Tel.: +86 571 87676357
Fax: +86 571 87676226
0000-0003-4323-7625

Current approaches for traceability and localization of water pollution primarily encompass fixed monitoring stations, manual emergency response, and single unmanned surface vessel (USV) systems [7, 8]. Fixed monitoring stations rely on a pre-established network to collect multidimensional water quality parameters, utilizing numerical modeling or Bayesian statistics to infer pollutant distribution and emission intensity [9, 10]. However, this approach is limited by the coverage density of the monitoring network, often resulting in missed detection of sudden pollution events in unmonitored areas [11]. Additionally, high deployment and maintenance costs, along with reliance on river hydrodynamic models, yield only approximate search ranges [12]. Manual emergency methods are labor-intensive and necessitate exhaustive inspections of potential emission points throughout the entire basin. This results in resource-intensive operations that are inefficient and pose safety risks to personnel [13-15]. A single USV employs sensors to track and locate pollution sources through iterative algorithms and concentration gradients, but its limited coverage and inability to integrate distributed multi-point sensing data hinder search efficiency [16-18].

In summary, current technologies for water pollution traceability encounter limitations in localization accuracy and search capabilities. This paper proposes a multi-USV approach that utilizes simultaneous multi-point pollutant monitoring and spatial location data, enabling coordinated USVs to precisely identify pollution sources through algorithmic optimization. The system provides rapid response capabilities for sudden contamination events, offering practical methodologies for emergency response agencies.

Materials and Methods

The Basic Wolf Pack Algorithm

Introduction to the Basic Wolf Pack Algorithm

The wolf pack algorithm (WPA), proposed by Wu et al. [19] in 2012, is a swarm intelligence optimization algorithm inspired by the social hierarchy and hunting strategies of wolves. Wolf packs demonstrate a structured division of labor, cooperative hunting, and adaptive prey distribution behaviors that have evolved for survival in harsh environments. WPA encapsulates three fundamental biological principles: wolf pack roles, collective foraging behaviors, and adaptive position updating rules, translating these into an optimization framework [20]. The following sections detail the algorithm's implementation, including wolf pack roles, and cooperative mechanisms.

1. Wolf Pack Roles

The WPA abstracts three wolf roles that collectively optimize search performance.

The head wolf plays a crucial role in decision-making and directing the hunting behavior of the pack, synthesizing information to facilitate swift prey capture. The fierce wolves carry out the head wolf's directives to initiate attacks, while also exhibiting autonomous movement when not actively commanded. Meanwhile, probing wolves extend the hunting territory by independently navigating towards areas that exhibit the most significant signs of prey activity.

This collaborative mechanism is illustrated in Fig. 1, with the following sections providing detailed explanations of each role's specific function within the wolf pack hierarchy.

2. Cooperative Mechanisms

Prior to detailing the wolves' collaborative hunting strategy, we establish key definitions. Each wolf perceives prey trace intensity through the objective function $Y_i = f(X_i)$, where Y_i represents individual i's fitness value at position X_i.

(1) Head Wolf Selection

The wolf with the optimal Y_i within the initial random population is designated as the head wolf, a position that is reelected in each iteration. If multiple wolves attain equally optimal values, selection among these candidates is random. The head wolf is exempt from participating in three intelligent behaviors: roaming, summoning, and siege. The fitness value at the head wolf's position is denoted as Y_{lead}.

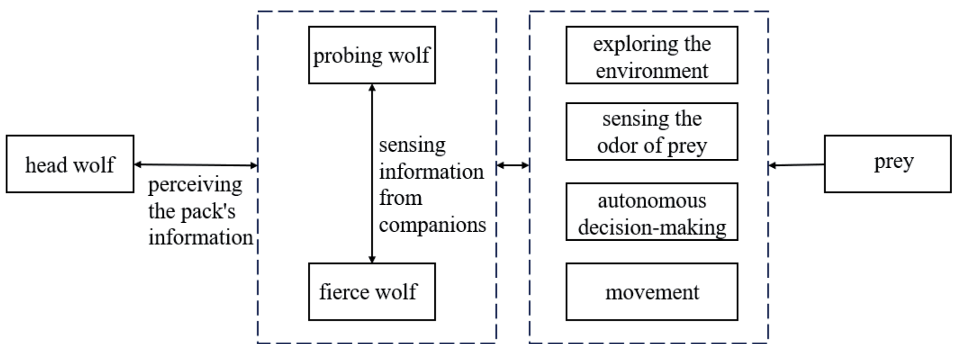

Fig. 1. Wolf Pack Character Collaboration.

(2) Probing Wolf Roaming

Top T_{num} wolves, excluding the head wolf, are designated as probing wolves, based on a probing ratio. Each probing wolf calculates its current fitness value, denoted as Y_i. A comparison is then made between Y_i and Y_{lead}.

When $Y_i > Y_{lead}$, the probing wolf takes over as the head wolf and issues a summoning call. Otherwise, it engages in roaming behavior until it either surpasses Y_{lead} or reaches the maximum threshold T_{max}. During this process, each probing wolf explores h directions with a $step_a$ size, returning to the origin position before moving toward the highest odor concentration. This positional update mechanism is formalized in Eq. (1):

$$x_{id}^{p} = x_{id} + \sin(2\pi \times p/h) \times step_a^d \tag{1}$$

Where x_{id} represents the position of the i-th probing wolf in the d-th dimension, h is the direction of the probing wolf roaming, p = 1,2,3...h. $step_a^{\,d}$ is the step size of roaming.

(3) Summoning Mechanism

When summoned by the head wolf, fierce wolves advance toward its position with $step_b$. Each fierce wolf evaluates its current fitness value Y_i against Y_{lead} to determine its behavioral response. The position update follows Eq. (2):

$$x_{id}^{k+1} = x_{id}^{k} + step_b^d \cdot (g_d^k - x_{id}^k)/|g_d^k - x_{id}^k| \tag{2}$$

Where $step_a^{\,d}$ is the movement step size and $g_d^{\,k}$ denotes the spatial location of the k-th generation head wolf in the d-th dimension.

When $Y_i > Y_{lead}$, the probing wolf assumes head wolf status and issues a summoning call. Otherwise, fierce wolf i continues approaching until the distance is less than d_{near}, and the distance of d_{near} is as in Eq. (3):

$$d_{near} = \frac{1}{D \cdot w} \cdot \sum_{d=1}^{D} |\max_d - \min_d| \tag{3}$$

The critical distance d_{near} is determined by the distance determination factor ω. Increasing ω enhances algorithm convergence speed, but beyond a reasonable threshold, hinders precise prey localization by the probing wolves. Here, d-th represents the dimension index with valid range [$\min_d$, $\max_d$] , and D is the total optimization variables.

(4) Siege Behavior

During the siege phase, fierce wolves that approach the prey coordinate with probing wolves to execute their strategy. The head wolf's position indicates the location of the prey. For the k-th generation wolf pack, the prey's position in d-dimensional space is x_d, the fierce wolves' positions during siege are governed by Eq. (4):

$$x_{id}^{k+1} = x_{id}^{k} + \lambda \cdot step_c^d \cdot |G_d^k - x_{id}^k| \tag{4}$$

Where $step_c^{\,d}$ is the attack step size and λ is a random number distributed between [-1,1]. The fierce wolf maintains its current position if it detects that the prey odor is weaker than its previous value. Otherwise, it updates its location.

These behavioral mechanisms (summoning, siege, and roaming) maintain the step size relationship defined in Eq. (5):

$$step_a^d = step_b^d/2 = 2 \cdot step_c^d = |\max_d - \min_d|/s \tag{5}$$

The step factor S regulates optimization granularity by controlling precision in solution space exploration.

(5) The Rule of Survival of the Fittest

The wolf pack implements a survival-of-the-fittest mechanism by removing the R wolves with the worst fitness values. While increasing R results in a global search, setting it too high may degrade search efficiency through excessive randomization. R is taken as a random integer between [$n/(2\times\beta)$, n/β] and β is the group update proportion factor.

3. Wolf Pack Algorithm Application and Analysis

The WPA effectively mimics natural wolf hunting behaviors, including head wolf leadership, probing wolf exploration, fierce wolf pursuit, and collective prey sieging, to achieve balanced global exploration and local exploitation [21, 22]. However, when applied to water pollution traceability tasks, this algorithm exhibits limitations that impair its performance.

(1) The WPA utilizes a fixed step size S that cannot dynamically adjust search steps based on pollutant concentration gradients. This rigidity presents two significant limitations: first, when pollutant concentrations are low and distant from the source, the algorithm is unable to increase its search speed; conversely, when concentrations are high and close to the source, it fails to decrease the step size. Additionally, the fixed step restricts the algorithm's capacity to escape local optima, ultimately undermining both traceability accuracy and operational efficiency.

(2) The WPA emulates the process of natural selection by removing the least fit individuals. However, in the context of traceability for water pollution using USVs, this approach results in random reassignment of positions following individual removal. Consequently, this diminishes search efficiency and reduces overall resource utilization.

The Improved Wolf Pack Algorithm

To address the limitations of the WPA in water pollution traceability, this study proposes an Improved Wolf Pack Algorithm (IWPA) featuring an improved search step and a survival-of-the-fittest mechanism, significantly enhancing search efficiency and localization accuracy.

Improved Search Step

The IWPA proposes a dynamic step adjustment mechanism that responds to real-time pollutant concentration feedback. This mechanism establishes a nonlinear mapping between pollutant concentration C and step size factor S, as formalized in Eq. (6):

$$S(i)=S_{\max}\cdot e^{-n\cdot\frac{C(i)}{C_{\max}}}+S_{\min}\cdot\left(1-e^{-n\cdot\frac{C(i)}{C_{\max}}}\right) \tag{6}$$

Step factor S is within bounds $[S_{min}, S_{max}]$, where $S(i)$ dynamically adjusts based on the i-th USV detected concentration $C(i)$ relative to the population's maximum C_{max}, the concentration sensitivity coefficient n controls the rate of step decay. As $C(i)\to 0$, $S(i)\to S_{max}$, realizing rapid global exploration. Conversely, as $C(i)\to C_{max}$, $S(i)\to S_{min}$, initiating localized fine search.

Eq. (7) demonstrates that the step size decreases monotonically as concentration increases, which aligns with the search process evolving from coarse to fine.

$$\frac{\partial S(t)}{\partial C(t)}=-\frac{n}{C_{\max}}(S_{\max}-S_{\min})\cdot e^{-n\frac{C(t)}{C_{\max}}} \tag{7}$$

The IWPA employs adaptive step sizing to mitigate the search inertia caused by the fixed step size, thereby facilitating escape from local optima. In regions of high concentration, smaller step sizes allow for a more refined search process, enabling precise localization of pollution sources.

Improved Survival-of-the-Fittest Mechanism

The Shannon-Wiener diversity index was introduced to optimize population distribution [23], as shown in Eq. (8).

$$D=-\sum_{i=1}^{M}\frac{n_i}{N}\ln\left(\frac{n_i}{N}\right) \tag{8}$$

where M is the number of character categories, N is the total population size, n_i denotes the individuals within the i-th population category, and D represents the population diversity index.

$$\begin{cases} D_{min}(N)=0.8-0.1\cdot\ln(N/10) \\ D_{max}(N)=0.8+0.1\cdot\ln(N/10) \end{cases} \tag{9}$$

The population diversity index D is bounded within the range $[D_{min}(N), D_{max}(N)]$, with an adaptive threshold function for increasing population as described in Eq. (9). This function narrows the threshold interval as N decreases, thereby enhancing the sensitivity of small populations. The IWPA compares D with the dynamic threshold interval. When $D<D_{min}$, it increases the number of probing wolves to boost exploration, while when $D>D_{max}$, it reduces the number of probing wolves to prevent overexploitation.

During the adjustment phase of probing wolves' count, an adjustment quantity Δ_{adj} is introduced to ensure sufficient intensity in small populations, as defined in Eq. (10). The effective parameter base N_{eff} is defined in Eq. (11), which ensures the strength. A random factor is presented in Eq. (12) and introduces non-deterministic perturbations to avoid local stiffness. The adjustment direction is determined by $sign(D_0-D)$, and the magnitude is determined by $[\eta\cdot N_{eff}]$, enabling adaptive and smooth changes in population size.

$$\Delta_{adj}=sign(D_0-D)\cdot[\eta\cdot N_{eff}] \tag{10}$$

$$N_{eff}=\max(N,5) \tag{11}$$

$$\eta\sim U(0,0.2) \tag{12}$$

$$Q_{bound}=\begin{cases}[2,N-2] & 3\leqslant N\leqslant 5\\ [\lfloor 0.3\cdot N\rfloor,\lfloor 0.4\cdot N\rfloor] & N>5\end{cases} \tag{13}$$

Q_{bound} is the boundary for probing wolves. After calculating the adjustment amount, a truncation process is applied to the adjusted probing wolves count Q, as shown in Eq. (13). For $3\le N\le 5$, the lower bound is raised to maintain exploration capacity. For $N>5$, proportional constraints balance exploration and exploitation. For $N=3$, the number of head wolves is fixed at 1, the number of probing wolves is fixed at 1, and the number of follower wolves at 1. The algorithm is skipped when $N<3$ due to insufficient population.

This modification avoids random position reassignment caused by the "death" of an individual and ensures maximum effectiveness of the multi-USV formation. Dynamic population planning enhances the balance between global exploration and local exploitation in water pollution traceability, thereby improving mission success rates.

Process for the Improved Wolf Pack Algorithm

The following are the specific steps of the IWPA:

Step 1: Parameter configuration and initialization. Set wolf pack size N, maximum iterations k_{max}, roaming threshold T_{max}, and distance factor w. Initialize dynamic step parameters: S_{max}, S_{min}, and sensitivity coefficient n. Calculate the diversity threshold according to Eq. (6). Generate the initial location X_i and evaluate pollutant concentration $C(t)$ as fitness value.

Step 2: Dynamic step adjustment. Adjust each wolf's step factor based on $C(t)$, as defined in Eq. (2-6). If $C(t)\to 0$, $S(t)\to S_{max}$, perform large-scale fast exploration, when $C(t)\to C(max)$, $S(t)\to S(min)$, perform fine-grained local exploration.

Step 3: Dynamic calculation of probing wolf count. Compute D according to Eq. (2). If $D<D_{min}(N)$, compute positive adjustment to increase probing wolf count. If $D>D_{max}(N)$, compute negative adjustment to decrease probing wolf count. Constrain the probing wolf count according to Eq. (13). For $N = 3$, fix probing wolves at $Q = 1$.

Step 4: Head wolf selection and probing wolf behavior. Select the individual with the highest fitness as head wolf, the top Q others are chosen as probing wolves. Each probing wolf explores until $Y_i>Y_{lead}$ or the detection count reaches T_{max}, then proceeds to Step 5.

Step 5: Fierce wolf attack. Fierce wolves move towards the target region based on Eq. (2). If $Y_i>Y_{lead}$, replace head wolf and activate summoning; if $Y_i\leq Y_{lead}$ and $d_{is}\leq d_{near}$, enter siege phase.

Step 6: Group siege and position update. Besieging wolves update positions using Eq. (4), tightening the encirclement. Recalculate D to guide the probing wolf in the next iteration.

Step 7: Termination check. Terminate and output X_{lead} as the estimated source if any of the following conditions are met: (1) iterations reach k_{max}; (2) sampling deviation stays below threshold for n_{time} times; (3) detection exceeds C_{max}. Otherwise, return to Step 2.

Simulation Environment Construction

After algorithmic improvements, a rigorous experimental program is essential for validation [24]. While real-world tests demonstrate practical performance, simulating diverse scenarios in the early research stage is crucial for evaluating the algorithm's feasibility and efficiency [25]. Therefore, constructing a simulation testing environment is vital for validating the IWPA and supporting subsequent experiments.

Two-Dimensional Water Quality Dispersion Modeling Studies

Water quality modeling is a vital tool for predicting and evaluating the trends and impacts of water pollution. It supports the analysis of spatial and temporal variations in pollutant diffusion and simulates transport processes [26-28]. Based on mass conservation, the model uses transport and transformation equations.

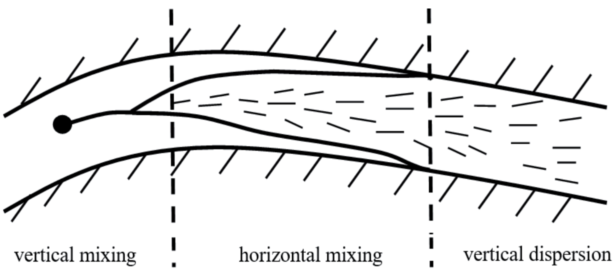

Fig. 2. Three diffusion processes of pollutants across water bodies.

Once pollutants are discharged, they undergo diffusion in three stages: vertical mixing, horizontal mixing, and vertical dispersion, as illustrated in Fig. 2.

In most inland shallow rivers, vertical mixing occurs much faster than lateral mixing and is often considered instantaneous, thus omitted from temporal calculations. Only lateral mixing and vertical dispersion are typically accounted for. This study focuses on flow direction and mass concentration variations across lateral sections. A two-dimensional water quality diffusion model is adopted, as expressed in Eq. (14).

$$\frac{\partial C}{\partial t}+u\frac{\partial C}{\partial x}+v\frac{\partial C}{\partial y}=D_x\frac{\partial^2 C}{\partial x^2}+D_y\frac{\partial^2 C}{\partial y^2}-kC+\sum S \tag{14}$$

In this two-dimensional water quality model, the parameters are defined as follows: C is pollutant concentration (mg/L); t is time (s); x and y are the longitudinal and transverse distance from the pollution source to the calculation point (m); u and v are the flow velocity components in the x and y directions (m/s); D_x and D_y are the dispersion coefficients (m²/s); k is the degradation coefficient (s^{-1}); and $\sum S$ represents the sum of all pollution sources within the domain.

This study considers far-bank and boundary reflections but neglects riverbed reflections.

Simulation Experiment Concentration Field Construction

Based on the two-dimensional water quality diffusion model, a simulation environment was constructed by setting appropriate parameters: river width B = 1000 m, near-shore distance b = 20 m, river depth h = 3 m, flow velocities u = 0.5 m/s and v = 0.01 m/s, diffusion coefficient D_x = 0.5 m²/s and D_y = 0.2 m²/s, degradation coefficient k = 0.0423 h^{-1}, background pollutant concentration C = 0 mg/L and an emission duration of 500 s. Crucially, considering the sensor's limit of detection and the need to filter ambient noise, the minimum operational threshold for the IWPA to initiate a trace was set at $C_{threshold}$ = 0.5 mg/L. MATLAB was employed to construct and simulate the two-dimensional diffusion model for a single pollutant source. The river boundary was delineated based on a central reference point and interpolated using the width parameter. Then, the pollutant concentration field was computed using the previously derived analytical expressions for concentration increments, and the simulation environment was thereby established.

The IWPA was verified in the simulated concentration field, confirming its accurate tracking of the multi-USV trajectory, as shown in Fig. 3.

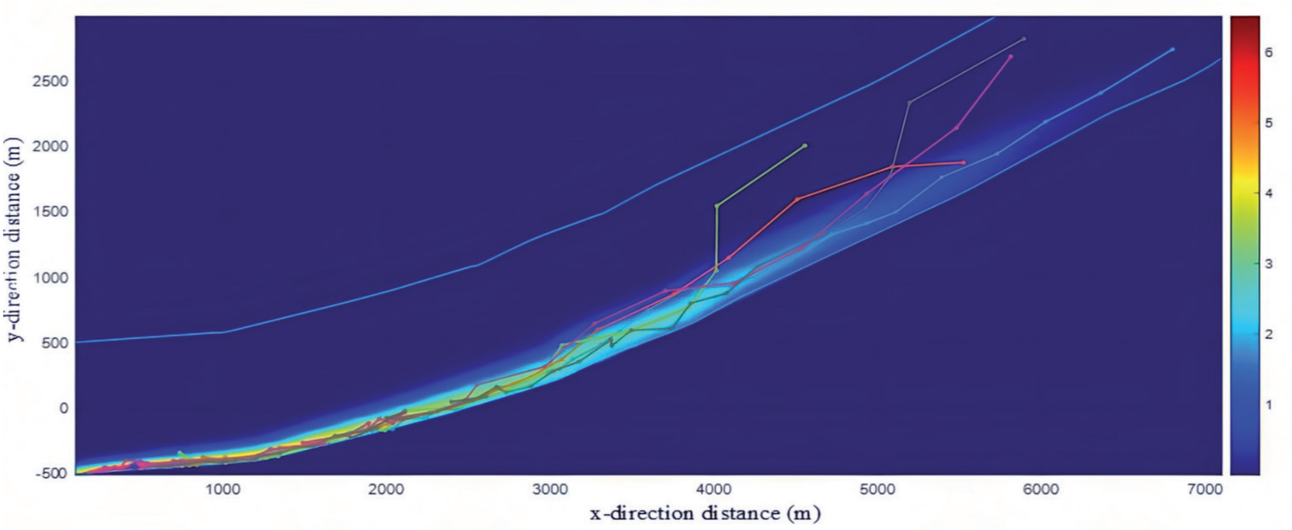

Fig. 3. The IWPA trajectory.

Results and Discussion

Simulation Results and Analysis of Water Pollution Traceability

Experimental Setup and Parameter Configuration

To evaluate the performance of the proposed IWPA, numerical simulations and laboratory experiments were conducted. The initialization of algorithmic hyperparameters is summarized in Table 1.

Algorithm Performance Evaluation Metrics

In evaluating the algorithm performance, this paper employs three metrics: localization success rate, average localization error, and average number of iterations.

Localization success rate refers to the proportion of all simulation experiments in which the pollution source is accurately identified within a 10-meter error margin. A higher success rate indicates superior algorithm performance. Average localization error represents the mean deviation between the identified pollution source and its true position across all successful experiments. A smaller average error distance signifies enhanced algorithm performance. Average number of iterations denotes the mean number of iterations required for all successful localization experiments. A lower average iteration count reflects greater algorithm efficiency.

Simulation Experiments and Analysis

In this paper, Particle Swarm Optimization (PSO), WPA, and IWPA are applied in the traceability simulation environment described in the chapter 'Simulation Experiment Concentration Field'.

A comparative framework is designed to assess their performance in terms of localization success rate, average number of iterations, and the average localization error under various conditions.

The simulation experiments first investigate the impact of the number of USVs on localization performance. Increasing the number of USVs enhances the spatial coverage and information density. However, it also raises coordination complexity, potentially reducing system efficiency. Subsequently, the influence of river hydraulic parameters is examined, where the pollution emission rate is varied between 500 and 2500 g/s,

Table 1. Hyperparameter settings for the IWPA algorithm.

Symbol	Parameter description	Simulation value	Experiment value	Reference
N	Population size	5	3	Task complexity and hardware limits [22]
n	Sensitivity coefficient	0.8	0.8	Convergence sensitivity analysis [22]
Q	Probing wolves count	3	1	Regulated by Eq. (13) to maintain exploration
S_{max}	Maximum step size	10 m	0.5 m	Scaled to search area dimensions
S_{min}	Minimum step size	1 m	0.1 m	Scaled to search area dimensions
k_{max}	Maximum iterations	100	100	Sufficient for convergence
w	Distance factor	2	0.2	Based on sensor range

Table 2. Effect of USV number on water pollution traceability simulation.

Number of USVs (ships)	Arithmetic	Success rate (%)	Average number of iterations (times)	Average localization error (m)
3	PSO	55.8	149.7	2.63
	WPA	65.1	132.4	2.25
	IWPA	76.5	109.2	1.52
4	PSO	60.2	142.7	2.35
	WPA	71.4	125.6	1.96
	IWPA	86.5	104.2	1.02
5	PSO	70.2	121.5	1.75
	WPA	82.4	97.8	1.43
	IWPA	97.3	75.3	0.41
6	PSO	72.9	114.5	1.64
	WPA	84.5	88.7	1.28
	IWPA	98.1	68.3	0.32
7	PSO	76.4	105.2	1.51
	WPA	89.6	83.1	1.22
	IWPA	100.0	61.4	0.28
8	PSO	82.3	96.5	1.28
	WPA	90.2	78.5	1.12
	IWPA	100.0	54.3	0.18
9	IWPA	100.0	54.3	0.18
	PSO	84.5	92.8	1.35
	WPA	90.2	78.5	1.12

Note: The experimental data are analyzed in terms of success rate, average number of iterations, and average localization error.

and the longitudinal flow velocity is set between 1.5 and 4.5 m/s.

A control variable method is adopted: when analyzing the influence of the number of USVs, hydraulic parameters are fixed; when investigating hydraulic conditions, the number of USVs remains constant.

1. Impact of the Number of USVs on Algorithm Performance

To assess the influence of the number of USVs on localization performance, hydraulic parameters were fixed at an emission rate of 1500 g/s and flow velocity of 3 m/s. The number of USVs varied from 3 to 10, under constant hydraulic conditions. 8 experimental groups were conducted, each running the algorithms 100 times. Results are shown in Table 2.

Fig. 4 shows the success rates of PSO, WPA, and IWPA under varying numbers of USVs. At 3 USVs, the IWPA achieves a success rate of 76.5%, which outperforms WPA's 65.1% and PSO's 55.8%. This demonstrates that dynamic role allocation effectively improves the utilization of swarm resources. With 7 USVs, the IWPA is the first to attain a 100% success rate and maintains this up to 10 USVs. The WPA stabilizes around 90.0%, showing slower gains beyond 7 USVs, while PSO gradually exceeds 80.0%.

Fig. 5 depicts the average number of iterations of PSO, WPA, and IWPA as the number of USVs varies. Beyond 6 USVs, the three algorithms exhibit a fluctuating trend. The IWPA demonstrates the fastest convergence speed, fluctuating between 59.1 and 68.3 iterations. Its average number of iterations drops from 109.2 with 3 USVs to 52.1 with 10 USVs, representing a reduction of 52.3%. In contrast, WPA reduces by 42.7% but shows limited efficiency gains, merely a 26.8% drop from 7 to 10 USVs due to its fixed step size and static population allocation. PSO decreases from 149.7 to 89.4 iterations, a decrease of 40.2%, with slowed improvement between 5 and 6 USVs.

Fig. 6 illustrates the average localization error of PSO, WPA, and IWPA across varying numbers of USVs. The IWPA demonstrates the highest localization accuracy. The average localization error of the IWPA decreases significantly, from 1.52 m at 3 USVs to just 0.12 m at 10 USVs. The WPA ranks second, showing a gradual downward trend and stabilizing around 1.10 m. In contrast, the PSO exhibits a decline in accuracy beyond 8 USVs, as its average localization error increases.

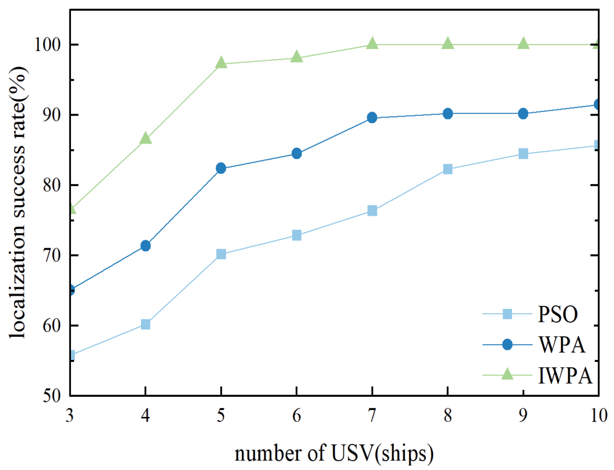

Fig. 4. Localization success rate of each algorithm varying with the number of USVs.

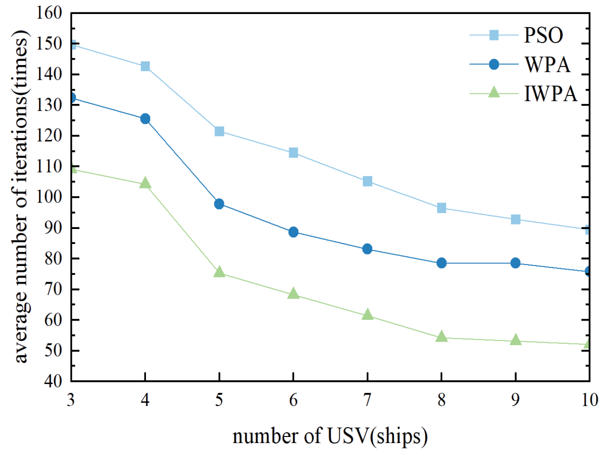

Fig. 5. Average number of iterations for each algorithm varying with the number of USVs.

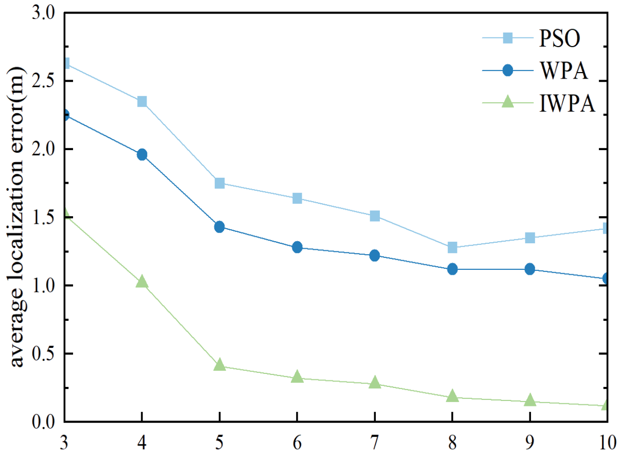

Fig. 6. Average localization error for each algorithm varying with the number of USVs.

From a comprehensive performance perspective, the IWPA outperforms both the WPA and the PSO across all three key metrics. With 7 USVs, the IWPA achieves a 100% success rate, maintains a stable average number of iterations between 52 and 68, and sustains average localization error below 0.3 m. These results demonstrate that the proposed enhancements improve success rate, localization error, and number of iterations. The WPA ranks second, with a maximum success rate of approximately 91.0% at 9 USVs; however, its average number of iterations and localization error are approximately 40% and 80% higher than IWPA. The PSO consistently underperforms in all metrics. Additionally, the experimental results indicate diminishing returns in algorithm performance beyond 5 USVs; the rate of improvement in success rate slows, while further gains in the number of iterations and the localization error become marginal. Therefore, deploying 5 to 6 USVs is recommended. At this configuration, the IWPA achieves a success rate exceeding 98%, offering optimal resource efficiency.

2. Impact of River Hydraulic Parameters on Algorithm Performance

To evaluate the effect of river hydraulic parameters on algorithm performance, the number of USVs was fixed at 5. Simulations varied two key parameters: source emission rate and longitudinal flow velocity. Specifically, emission rates were set at 500 g/s, 1500 g/s, and 2500 g/s, while longitudinal velocities were set at 1.5 m/s, 3.0 m/s, and 4.5 m/s, forming 9 experimental conditions. Each scenario was repeated 100 times per algorithm to ensure statistical reliability. Results are summarized in Table 3.

Fig. 7 illustrates the localization success of PSO, WPA, and IWPA under varying emission rates and flow velocities. As emission increased from 500 g/s to 2500 g/s, the success rate of the IWPA improved by 21.2%, benefiting from an enhanced concentration gradient. The PSO and the WPA improved by 33.4% and 25.7%, respectively, but with diminishing gains. Under the 500 g/s low-emission conditions, increasing flow velocity from 1.5 m/s to 4.5 m/s led to a 9.3% drop in the IWPA's success rate, whereas the PSO and the WPA decreased by 23.1% and 11.0%, respectively. This indicates that the IWPA's dynamic step adjustment mechanism mitigates the challenges of narrow, fast-moving pollutant plumes. Even under extreme conditions, it maintained a success rate above 70%, outperforming the WPA by 15.5%, highlighting its effective balance of exploration and stability.

Fig. 8 illustrates the average number of iterations of the PSO, WPA, and IWPA algorithms under varying emission rates and flow velocities. Emission rate and longitudinal flow velocity significantly affect algorithm convergence efficiency. As the emission increases from 500 g/s to 2500 g/s, the IWPA's iterations decrease by 51.7% – for instance, at a flow rate of 1.5 m/s, the number of iterations drops from 89.6 to 42.1. This demonstrates the effectiveness of its dynamic step adjustment

Table 3. Experimental results of water pollution traceability under varying hydraulic parameters.

Emission rate (g/s)	Longitudinal flow velocity (m/s)	Arithmetic	Success rate (%)	Average number of iterations (times)	Average localization error (m)
500	1.5	PSO	56.3	148.7	3.92
		WPA	68.5	115.2	2.68
		IWPA	82.4	89.6	1.74
500	3	PSO	49.8	162.4	4.35
		WPA	63.1	127.8	3.02
		IWPA	78.9	94.3	2.15
	4.5	PSO	43.2	178.9	5.17
		WPA	57.6	141.5	3.89
		IWPA	73.1	107.6	2.73
1500	1.5	PSO	72.5	112.4	2.14
		WPA	85.7	84.3	1.58
		IWPA	96.8	61.2	0.63
	3	PSO	70.2	121.5	1.75
		WPA	82.4	97.8	1.43
		IWPA	97.3	75.3	0.41
	4.5	PSO	65.9	136.7	2.48
		WPA	78.1	109.4	1.92
		IWPA	94.5	82.9	0.87
2500	1.5	PSO	89.7	78.6	1.25
		WPA	94.2	57.3	0.82
		IWPA	99.6	42.1	0.19
	3	PSO	86.4	84.9	1.38
		WPA	92.7	63.8	0.95
		IWPA	99.1	45.6	0.24
	4.5	PSO	81.5	93.2	1.67
		WPA	89.4	72.4	1.14
		IWPA	98.3	51.8	0.32

Note: The experimental data were analyzed in terms of success rate, average number of iterations, and average localization error.

mechanism in a high concentration gradient. PSO and WPA decrease by 47.3% and 50.2%, respectively, though the reduction rate slows as flow velocity increases. Under the extreme condition of 500 g/s emission rate and longitudinal flow velocity of 4.5 m/s, IWPA achieves 23.9% fewer iterations than the WPA and 40.0% fewer than the PSO. These results confirm IWPA's adaptability to narrow or rapidly dispersed plumes via dynamic step adjustment, while its balanced role allocation mitigates convergence redundancy and enhances overall search efficiency.

Fig. 9 illustrates the average localization error of the PSO, WPA, and IWPA under varying emission rates and longitudinal velocities. IWPA exhibits stronger robustness under dynamic concentration gradients and flow velocity changes. At high emission rates, its fine-grained searches use small step sizes, reducing localization error by 74.7% to 80.8% compared to the WPA. For instance, at a flow velocity of 3 m/s, the localization error is as low as 0.24 m, highlighting its superior local optimization. Under the condition of low emission and high flow velocity, its dynamic step-size adjustment and diversity index control reduce error by 29.8% over WPA and 47.2% over PSO, mitigating drift from fast flow. Even in extreme conditions, IWPA keeps error within 3 m, improving stability by 42.1% to 58.9% over the WPA. These results confirm its dual optimization in both search precision and environmental adaptability.

Experimental Evaluation and Analysis

Preliminary Experimental Preparations

Tracer Selection: Sodium chloride (NaCl) solutions of varying concentrations were selected as tracers.

USV water quality sensing system: A DJS-1 electrode-based conductivity sensor module was integrated into the USVs for pollutant detection.

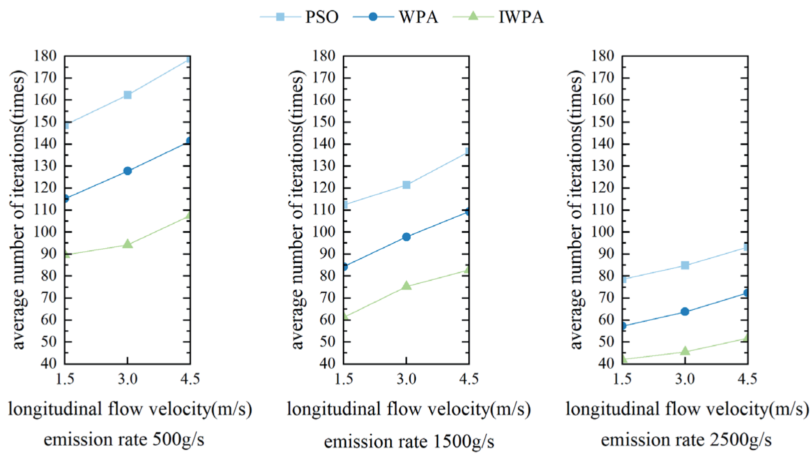

Fig. 7. Average localization success rates of algorithms under varying flow velocities and emission rates.

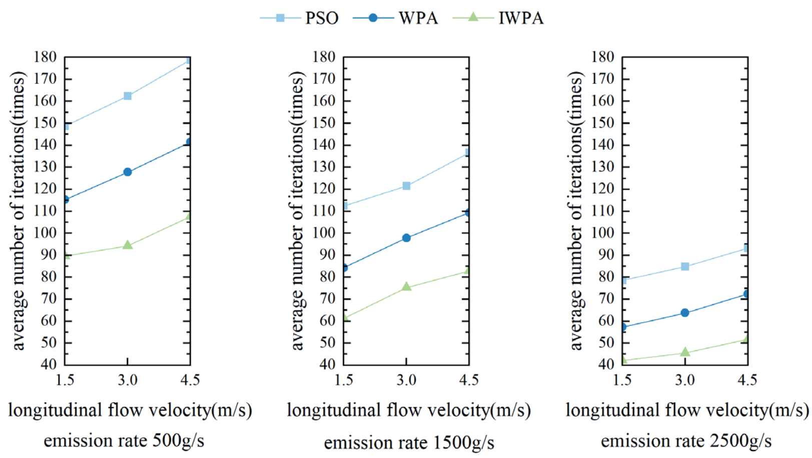

Fig. 8. Average number of iterations for algorithms under varying longitudinal flow velocities and emission rates.

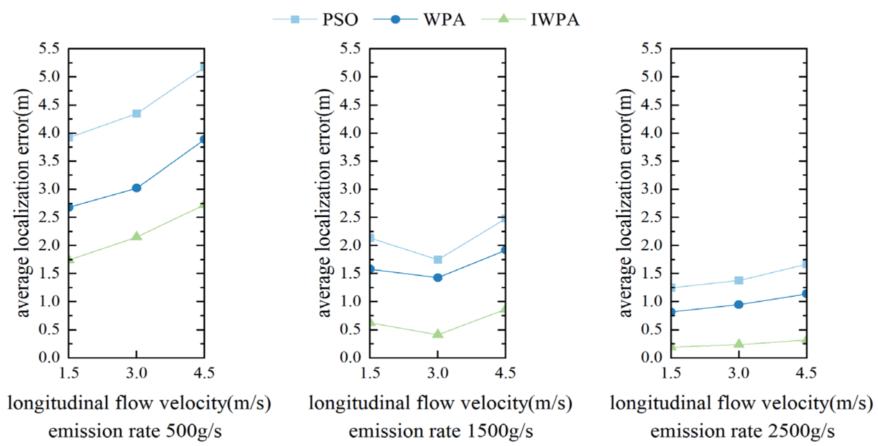

Fig. 9. Average localization error of algorithms under varying longitudinal flow velocities and emission rates.

Standard reference instrument: Conductivity measurements were calibrated using the LH-TDS9 portable sensor developed by Luheng Bio.

Experimental platform: A laboratory-developed multi-USV traceability platform was employed, supporting algorithm integration and testing in a controlled indoor environment.

Experimental environment: Experiments were conducted in a water tank (400 cm × 200 cm × 50 cm) equipped with a downstream outlet for flow regulation

Fig. 10. On-site photographs of the USV-Based Pollution Source traceability experiment.

and an auxiliary reservoir for inflow control. The tank was placed in an open area with strong GPS reception and minimal magnetic interference to ensure stable operating conditions.

Experimental Procedures

(1) Prepare an NaCl solution with a conductivity of 2100 μS/cm as the tracer and pour it into the reservoir tank.

(2) Measure the initial conductivity of the water in the tank, which is recorded as 46 μS/cm.

(3) Simultaneously open the reservoir tank and outlet valves and set both flow rates to 0.2 L/s to ensure the NaCl solution enters into the flowing water at a controlled rate.

(4) After 300 s of continuous emission, close both valves. Collect water samples at each designated point using the standard conductivity sensor at a depth of 5 cm. Record the conductivity at each point. The point with the highest conductivity, corresponding to the reservoir tank outlet, is identified as the pollution source for the traceability task.

(5) Randomly deploy USVs near the outlet. Use the multi-USV control interface to manually disperse their initial positions. Run the source-tracking algorithm and wait for localization to be completed. Repeat the experiment five times to ensure consistency and statistical reliability. The experimental process is illustrated in Fig. 10.

Table 4. Experimental record of water pollution traceability.

Experimental group	Traceability status	Number of iterations	Localization error
1	Success	37 iterations	17 cm
2	Failure	-	-
3	Success	42 iterations	13 cm
4	Success	38 iterations	37 cm
5	Success	50 iterations	41 cm

Preliminary Experimental Preparations

If the traceability USV platform localizes to within 50 cm of the NaCl emission point within 50 iterations, the attempt is considered a successful localization. The experimental results are summarized in Table 4.

Table 4 presents the results of the tracing conducted in each experiment. The second trial encountered a failure due to a malfunction in RTK positioning on one USV, which led to significant localization errors and a system-wide freeze. Among the successful trials, relatively high localization errors were noted, likely attributable to the onboard sensor exceeding its detection limit of 2000 μS/cm, as peak conductivity reached 2156 μS/cm. Out of the five experiments conducted, four successfully identified the pollution source, resulting in an overall success rate of 80%. These findings validate both the feasibility of IWPA for multi-USV coordination in source tracing and demonstrate the operational reliability of the tracing platform.

The failure in Trial 2 underscores the necessity of system robustness. The results confirm that the decentralized nature of IWPA provides inherent resilience; the loss of a single USV's positioning data does not lead to mission failure, as the remaining formation can autonomously re-configure its search strategy to compensate for the missing node.

Conclusions

Amid the growing challenges of water scarcity and pollution in China, rapid traceability and emergency response to sudden water pollution incidents have become critical. This study proposes a multi-USV water pollution traceability and localization method based on the IWPA, addressing the limitations in existing traceability technologies, including low localization accuracy, insufficient search efficiency, and high costs of traditional positioning systems.

The IWPA introduces two core improvements to the WPA, specifically tailored for water pollution traceability. First, a dynamic step adjustment mechanism establishes a nonlinear mapping between pollutant concentration and step size, allowing large steps for rapid exploration in low-concentration areas and enabling small step sizes for fine-grained search in high-concentration areas, effectively balancing global exploration and local exploitation. Second, a dynamic population planning mechanism, based on the Shannon-Wiener diversity index, dynamically adjusts the ratio of probing and fierce wolves, which avoids resource waste caused by traditional "survival of the fittest" rules and enhances population efficiency.

A two-dimensional diffusion-based water quality model was used to construct a simulation environment under variable hydraulic parameters. Simulation results demonstrate that the IWPA outperforms the PSO and the WPA in terms of localization success rate, average number of iterations, and average localization error. In a 5 USVs scenario, the IWPA achieves a 97.3% success rate with an average localization error of merely 0.41 m, representing gains of 15.9% and 71.3%, respectively, over the WPA.

Laboratory validation was performed using a controlled water tank equipped with NaCl tracers and multi-USV. In the 5 experimental trials, 4 successfully identified the pollution source, resulting in an 80.0% success rate, an average localization error of 27 cm, and the average number of iterations of 42. These results confirm the feasibility of the IWPA for real-world pollution source tracing and highlight the operational reliability of the multi-USV traceability platform.

Regarding the hardware limitations observed in experimental trials, such as sensor saturation at peak concentrations, the IWPA demonstrated significant robustness through its dynamic step mechanism. This feature maintains high search precision by transitioning to a refined search mode even when spatial gradient information is partially constrained by sensor limits. Future research will focus on integrating multi-range sensor fusion and adaptive sampling frequencies to further enhance the system's reliability and resolution in extreme pollution scenarios.

Regarding future work, the current multi-USV formation logic provides a solid foundation for multi-source traceability. Future research will explore dynamic population partitioning strategies to enable the simultaneous identification of multiple pollution sources in large-scale aquatic environments.

Acknowledgments

This research did not receive any specific grant from funding agencies in the public, commercial, or not-for-profit sectors.

AI Usage Disclosure Statement

During the preparation of this manuscript, the authors employed DeepSeek-V3 solely for English grammar and spelling checking of the initial manuscript and the responses to reviewer comments during the revision stage. All text modified by the AI tool was fully reviewed and manually proofread by the authors, and all statements, references, and data were carefully verified. No AI tool was used in research design, experimental setup, simulation coding, data analysis, result interpretation, or conclusion formulation; all experimental data were obtained independently by the author through simulation and experimentation, and AI was not involved in data generation, processing, or analysis, so all results are verifiable. All authors take full responsibility for the originality, accuracy, and integrity of all content in this manuscript.

Conflict of Interest

The authors declare no conflict of interest.

References

1. LI X., LI P., MU D., LIU J. Spatiotemporal evolution of water resource sustainability in Shaanxi (China) from 2010 to 2020 based on an adapted water resources ecological footprint model. Hydrological Sciences Journal, **69** (10), 1335, **2024**.
2. YANG D., YANG Y., XIA J. Hydrological cycle and water resources in a changing world: A review. Geography and Sustainability, **2** (2), 115, **2021**.
3. CHAWLA I., KARTHIKEYAN L., MISHRA A.K. A review of remote sensing applications for water security: Quantity, quality, and extremes. Journal of Hydrology, **585**, 124826, **2020**.
4. ZHOU F., BO Y., CIAIS P., DUMAS P., TANG Q., WANG X., LIU J., ZHENG C., POLCHER J., YIN Z., GUIMBERTEAU M., PENG S., OTTLE C., ZHAO X., ZHAO J., TAN Q., CHEN L., SHEN H., YANG H., PIAO S., WANG H., WADA Y. Deceleration of China's human water use and its key drivers. Proceedings of the National Academy of Sciences, **117** (14), 7702, **2020**.
5. LIAO R. Water scarcity assessment index from the realistic perspective of human basic water requirements. Environmental Sustainability Indicators, **22**, 100404, **2024**.
6. JAIN S., SRIVASTAVA A., KHADKE L., CHATTERJEE U., ELBELTAGI A. Global-scale water security and desertification management amidst climate change. Environmental Science Pollution Research, **31** (49), 58720, **2024**.
7. LIU Y., HARVEY C.M., HAMLYN F.E., LIU C. Bayesian estimation and reconstruction of marine surface contaminant dispersion. Science of the Total Environment, **907**, 167973, **2024**.
8. LUO X., YANG J. A survey on pollution monitoring using sensor networks in environment protection. Journal of Sensors, **2019** (1), 6271206, **2019**.
9. WU R., QIAN S.S., HAO F., CHENG H., ZHU D., ZHANG J. Modeling contaminant concentration distributions in China's centralized source waters. Environmental Science and Technology, **45** (14), 6041, **2011**.
10. ZHAO Y., SHARMA A., SIVAKUMAR B., MARSHALL L., WANG P., JIANG J. A Bayesian method for multi-pollution source water quality model and seasonal water quality management in river segments. Environmental Modelling and Software, **57**, 216, **2014**.
11. KONRAD C.P., ANDERSON S.W. A general approach for evaluating of the coverage, resolution, and representation of streamflow monitoring networks. Environmental Monitoring Assessment, **195** (10), 1256, **2023**.
12. DA SILVEIRA BARCELLOS D., DE SOUZA F.T. Optimization of water quality monitoring programs by data mining. Water Research, **221**, 118805, **2022**.
13. ZOU F., JIANG H., CHE E., WANG J., WU X. Quantitative evaluation of emergency shelters in mountainous areas

among multiple scenarios: Evidence from Biancheng, China. International Journal of Disaster Risk Reduction, **90**, 103665, **2023**.

14. WANG Y., ZHANG W., ENGEL B.A., PENG H., THELLER L., SHI Y., HU S. A fast mobile early warning system for water quality emergency risk in ungauged river basins. Environmental Modelling and Software, **73**, 76, **2015**.
15. YANG R., JIANG J., PANG T., YANG Z., HAN F., LI H., WANG H., ZHENG Y. Crucial time of emergency monitoring for reliable numerical pollution source identification. Water Research, **265**, 122303, **2024**.
16. SOTELO-TORRES F., ALVAREZ L.V., ROBERTS R.C. An unmanned surface vehicle (USV): Development of an autonomous boat with a sensor integration system for bathymetric surveys. Sensors, **23** (9), 4420, **2023**.
17. HUANG X. Improved 'infotaxis' algorithm-based cooperative multi-USV pollution source search approach in lake water environment. Symmetry, **12** (4), 549, **2020**.
18. SUDHA S.K.R., MISHRA D., HAMEED I.A. A coverage path planning approach for environmental monitoring using an unmanned surface vehicle. Ocean Engineering, **310**, 118645, **2024**.
19. WU H.-S., ZHANG F., WU L. New swarm intelligence algorithm-wolf pack algorithm. Systems Engineering and Electronics, **35** (11), 2430, **2013**.
20. XIU-WU Y., HAO Y., YONG L., REN-RONG X. A clustering routing algorithm based on wolf pack algorithm for heterogeneous wireless sensor networks. Computer Networks, **167**, 106994, **2020**.
21. WU H.-S., ZHANG F.-M. Wolf pack algorithm for unconstrained global optimization. Mathematical Problems in Engineering, **2014**, (1), 465082, **2014**.
22. CHEN X., CHENG F., LIU C., CHENG L., MAO Y. An improved Wolf pack algorithm for optimization problems: Design and evaluation. PLos One, **16** (8), e0254239, **2021**.
23. YONGBO C., YUESONG M., JIANQIAO Y., XIAOLONG S., NUO X. Three-dimensional unmanned aerial vehicle path planning using modified wolf pack search algorithm. Neurocomputing, **266**, 445, **2017**.
24. MING F., GONG W., WANG L., JIN Y. Constrained multi-objective optimization with deep reinforcement learning assisted operator selection. IEEE/CAA Journal of Automatica Sinica, **11** (4), 919, **2024**.
25. AMARAN S., SAHINIDIS N.V., SHARDA B., BURY S.J. Simulation optimization: a review of algorithms and applications. Annals of Operations Research, **240**, 351, **2016**.
26. CHO K.H., PACHEPSKY Y., LIGARAY M., KWON Y., KIM K.H. Data assimilation in surface water quality modeling: A review. Water Research, **186**, 116307, **2020**.
27. ALOTAIBI E., NASSIF N. Artificial intelligence in environmental monitoring: in-depth analysis. Discover Artificial Intelligence, **4** (1), 84, **2024**.
28. EJIGU M.T. Overview of water quality modeling. Cogent Engineering, **8** (1), 1891711, **2021**.